Nuclear Instruments and Methods in Physics Research A 1071 (2025) 170068

Contents lists available at ScienceDirect

Nuclear Inst. and Methods in Physics Research, A

journal homepage: www.elsevier.com/locate/nima

Full Length Article

Monte Carlo simulations towards the formation of a positronium coherent beam

M. Sacerdoti [a], V. Toso [b,c], G. Vinelli [d,e,f], M. Bayo [a,c], G. Rosi [d,e], L. Salvi [d,e,f], G.M. Tino [d,e,f], M. Giammarchi [c], R. Ferragut [a,c,*]

[a] L-NESS and Department of Physics, Politecnico di Milano, Via Anzani 42, 22100 Como, Italy
[b] Department of Physics, Università degli Studi di Milano, Via Celoria 16, 20133 Milano, Italy
[c] INFN, Sezione di Milano, Via Celoria 16, 20133 Milano, Italy
[d] Department of Physics and Astronomy, Università di Firenze, Via Sansone 1, 50019 Sesto Fiorentino, Italy
[e] INFN, Sezione di Firenze, Via Sansone 1, 50019 Sesto Fiorentino, Italy
[f] LENS, Via Nello Carrara 1, 50019 Sesto Fiorentino, Italy

ARTICLE INFO

Keywords:
Atomic beam
Positronium
Gravity
Antimatter

ABSTRACT

Positronium (Ps) has emerged as a promising test particle within the QUantum interferometry with Positrons, positronium and LASers (QUPLAS) project, which aims to measure for the first time the gravitational effect on Ps, the entirely leptonic atom comprising an electron and a positron. In this work, we present a Monte Carlo simulation to generate a mono-energetic and highly coherent Ps beam by creating a negative Ps ion (Ps^- consisting of two electrons and one positron) to be used in a Mach–Zehnder interferometer. We propose the equations to estimate the initial velocity distributions in the longitudinal and transversal directions of the Ps^- emitted from the target converter (positron/Ps^-) necessary for the Monte Carlo simulation. The resulting simulated device needs a very low divergence Ps beam at the interferometer entrance, for this reason an intensive positron beam is necessary, such as a high-flux electron LINAC. Subsequently, we utilize a Fabry–Perot IR laser cavity operating in CW at a wavelength of 1560 nm to selectively remove the extra electron. An alternative pulsed laser operating at a 3600 nm wavelength was studied to reduce broadening due to recoil and excitation. Here, we provide a Monte Carlo simulation to estimate the characteristics of the Ps beam, including its energy distribution and intensity profiles at two different temperatures (10 K and 300 K). Despite the limitations given by the assumptions mentioned in the text within the limit of our knowledge, these first simulation results obtained from our study will provide essential groundwork for future advancements in fundamental particles gravity measurements.

1. Introduction

Gravitational studies with antimatter systems are of paramount importance to address Physics at the Planck scale, the current uppermost conceptual limit of validity of our physical theories. Quantum Gravity effects might in fact induce violation of the two basic symmetries that relate Quantum Mechanics and the General Relativity: the Einstein Equivalence Principle (EEP) and the CPT (Charge-Parity-Time) invariance. The most complete theoretical framework that includes the possibility of Lorentz violation (and therefore EEP and CPT violation) is the Standard Model Extension (SME) [1,2]. The SME includes all the Physics known in the form of the Standard Model and the General Relativity, while adding to the Lagrangian the possible spacetime operators violating Lorentz invariance. Recently, the ALPHA collaboration has shown that antihydrogen atoms behave in a way consistent with gravitational attraction to the Earth [3]. In this frame, research with positronium, the bound system of an electron and a positron, is particularly interesting, since (contrary to the antihydrogen case) positronium is a fundamental system composed by fermionic mass alone, with its binding energy insignificantly small compared to its mass. On the other hand, the antiproton mass is mostly due to the energy of the QCD color field, i.e. binding energy, instead of the mass of the elementary particles, i.e. gluons. Therefore, our proposal would involve the first measurement of the gravitational acceleration of elementary particles, i.e. leptons. In addition, the coefficients for Lorentz invariance violation are flavor-dependent [4]; for these reasons positronium gravitation constitutes an entirely new and independent window on Physics beyond the validity of our current best theories. For instance, in the frame of the SME, it has been shown that gravitation with positronium

* Corresponding author at: L-NESS and Department of Physics, Politecnico di Milano, Via Anzani 42, 22100 Como, Italy.
E-mail address: rafael.ferragut@polimi.it (R. Ferragut).

https://doi.org/10.1016/j.nima.2024.170068
Received 16 May 2024; Received in revised form 17 October 2024; Accepted 6 November 2024
Available online 18 November 2024

can address relevant physical parameters already at about the 10% accuracy level [4], regarding matter-antimatter symmetry.

Positronium (Ps) exists in the ground state in two sub-levels, according to the spins of the two particles: singlet called para-Ps with spin 0 and a lifetime of 0.125 ns and triplet called ortho-Ps with spin 1 and a lifetime of 142 ns. Para-Ps annihilates with the emission of two photons of 511 keV each while ortho-Ps emits at least three photons with a maximum energy of 511 keV each. Due to the short lifetime of para-Ps only ortho-Ps can be used in this experiment and Ps will always correspond to ortho-Ps in the remainder of this paper.

In a recent experiment, results were obtained with Ps transmittance through graphene layers employing a pulsed regime with a primary beam of the negative positronium ion, Ps^- [5]. This methodology has been developed by the Nagashima group in Tokyo in the last fifteen years [6]. Our proposal for gravitational measurements involves the use of a continuous regime version with a Ps^- primary beam, which is a remarkably ambitious challenge. This endeavor requires orders of statistical magnitude higher than the current version, as explained in more detail in the following sections, and requires study and simulations to optimize the complete system.

This work presents a Monte Carlo simulation for generating a monoenergetic and highly coherent Ps beam through the creation of a negative Ps^- ion [7]. The advantage of producing Ps through negative Ps^- ions, in contrast to Ps formed in meso-porous materials [8–10], is the ability to achieve a tunable and monoenergetic beam with low divergence and high coherence, making it well-suited for interferometric experiments. However, the drawback is the short Ps^- lifetime (479 ps [11]), necessitating the use of a very compact system to efficiently produce, accelerate, and focus the Ps^- beam using electrodes. Subsequently, a laser system selectively removes the extra electron to form the Ps beam. The Monte Carlo results lay essential groundwork for future advancements in fundamental studies, including Ps gravity measurements using a Large Momentum Transfer Mach–Zehnder interferometry [12–14].

2. Result and discussion

An effective positronium negative ion (Ps^-) producing target consists of a tungsten (W) coated with a sodium (Na) sub-monolayer, as demonstrated in the last two decades by Nagashima's group that produced and worked with a Ps^- beam. [7]. A Monte Carlo simulation was performed to quantify the Ps beam characteristics as a function of various factors such as Ps^- formation, temperature dependence of the converter target, guide and photo-detachment. For this purpose, we introduced a possible optimized velocity distribution for Ps^- emission, a miniaturized focusing and accelerating optics, and two possible laser photo-detachment systems.

2.1. Ps^- emission velocity

A velocity distribution of the Ps^- emitted from the target surface is hereby proposed. In general, there are many potential effects that could influence the velocity distribution of the emitted ions from the target surface with a negative work function (see for instance Ref. [15]). The thermal effect contribution given by the temperature of the emitter target is one of the most significant effects. Another effect that impacts the emission, especially visible in monocrystals, is the periodic lattice structure of the target and its electron energy distribution [16]. In fact, in the case of photoelectron emission, the angle-resolved photoemission spectroscopy (ARPES) technique to study crystalline solids is based on this principle. There is also evidence of this effect for the positronium emission with negative work function from aluminum (Al) single crystals [17]. Another effect, probably more relevant in semiconductors, is the excitation of electron–hole pairs. In fact, it could influence the scattering angles recently observed in semiconductors [18], which are higher than those observed in metals [19].

On the other hand, it is crucial to consider the surface topology and contamination that affect the directional emission of particles, often not considered in the literature. From the theoretical point of view the negative work function contributes with an emission component perpendicular to the surface. Therefore, the surface roughness increases the broadening of the angular distribution of the emission. For example, if only an effect of thermal contribution is expected for Ps in metals (see Refs. [19,20]), the combination of this effect with the surface roughness could be interpreted as a broadening of the angular distribution of emitted particles, which would appear to be emitted at higher effective temperatures.

Although Nagashima's group has studied Ps^- formation in both reflection and transmission geometries, there is still no estimation of the functional form for the initial Ps^- velocity distribution. Nevertheless, understanding these initial conditions is crucial for the accuracy of the Monte Carlo simulation proposed in this work. An approach based on the observed experimental results obtained in W, Ni, Cu and Al for positronium and positrons [19–22] emitted with negative work function is hereby proposed. Following this experimental evidence and considering "ideal" conditions such as a flat surface of the W target (coated with Na), thermal equilibrium between particle and phonons and negligible scattering effect, the velocity distribution is influenced by the negative work function and the thermal effect. We are aware that this is an idealized condition for calculating the necessary initial conditions of the Monte Carlo simulations and that the actual velocity distribution is likely to be wider. Nevertheless, this approach represents the first-ever proposal of a particle emission velocity distribution with a negative work function. It not only serves as a guide for optimizing ion emission conditions but also enables the design of optimized optics for beam guiding, as outlined in the following sections. The efficacy of this proposed distribution should be tested in the near future and potentially refined.

As shown later, the contribution of thermal energy has a non negligible effect on the propagation of atoms in the directions parallel to the surface of the W target (called x and y-directions or transversal direction, see Fig. 1 (a)). A classical two-dimensional Maxwell–Boltzmann distribution is proposed in this case, where the pre-exponential factor depends linearly on velocity:

$$f_T(v) = 2\alpha v \exp(-\alpha v^2), \tag{1}$$

where α is obtained by integrating Eq. (1) and depends on the target temperature T,

$$\alpha = \frac{1}{2}\frac{m_{Ps^-}}{kT} = \frac{3}{2}\frac{m_0}{kT}, \tag{2}$$

m_{Ps^-} and m_0 are the negative ion Ps^- and electron masses and k the Boltzmann constant.

The topic of particle emission in the direction perpendicular to the surface (called the z or longitudinal direction, see Fig. 1 (a)) with a negative work function is rarely addressed in the literature. However, some works deal with the emission of positrons with a negative work function to obtain energy distributions with experimental results [22]. They claim that the particles are directed similarly to a collimated beam of gas molecules effusing as in the Stern-Gerlach experiment, following a Maxwell–Boltzmann distribution. The proposed velocity distribution takes the following form,

$$g_L(v) = \beta\left(\frac{1}{2}mv^2 - \phi\right)^{3/2}\exp(-\alpha v^2), \tag{3}$$

Note that the exponent applied to the parenthesis is 3/2 to follow the pre-exponential tendency of v^3 proposed in Ref. [22]. Additionally, the negative work function ϕ is explicitly considered as the main contribution to the Ps^- ion initial kinetic energy in this longitudinal direction. The minimum permissible Ps^- kinetic energy is higher than the absolute value of ϕ. Although Eq. (3) has a simple functional form, it does not have a definite integral. Therefore, to obtain a reliable approximation of the beta function's dependence on temperature, it was necessary to normalize Eq. (3) by integrating it using a numerical

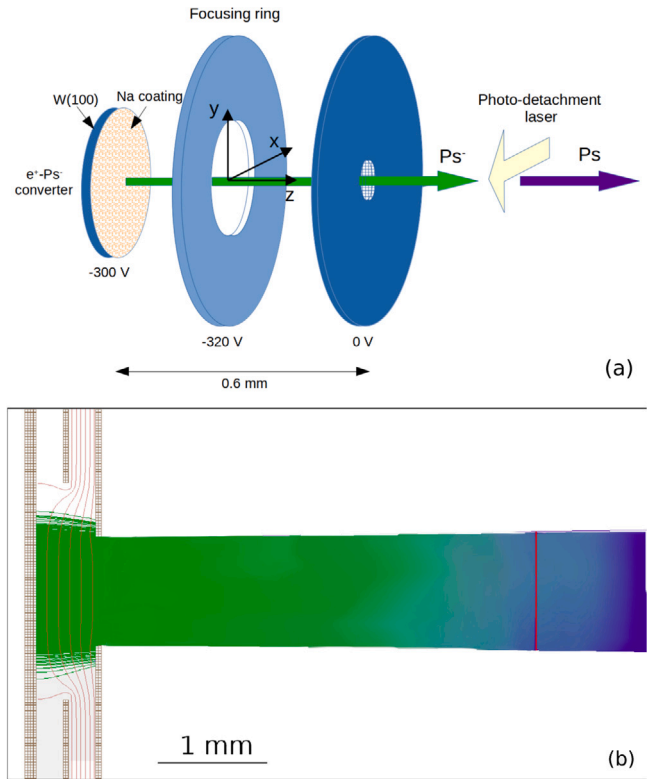

Fig. 1. (a) Schematic representation of the optics, not drawn to scale. (b) SIMION® simulated beam represented to scale. The electric field lines between the electrodes, shown as red lines, which follow a cylindrical symmetry, have been included. The green trajectories represent the Ps^- ion beam, while the violet trajectories represent the Ps beam after photo-detachment. Both Ps^- and Ps trajectories are plotted solely for visualization purposes, without considering their natural decay. The green/violet transition lines represent the photo-detachment interaction zone. The vertical red line corresponds to the initial position of the excitation and Mach–Zehnder interferometer stages (see Ref. [14]).

method at various temperatures. Considering the identified temperature effect and rearranging Eq. (3) to be implemented in the Monte Carlo simulation,

$$g_L(v) = c_z\alpha^2\left(\frac{\phi}{kT}\right)^{1/2}\left(v^2 - v_0^2\right)^{3/2}\exp\left[-\alpha\left(v^2 - v_0^2\right)\right] = c_z\alpha^2\left(\frac{\phi}{kT}\right)^{1/2}\delta v^3\exp\left(-\alpha\delta v^2\right) \quad (4)$$

where

$$v_0^2 = \frac{2}{3}\frac{\phi}{m_0}, \quad (5)$$

and

$$\delta v^2 = v^2 - v_0^2. \quad (6)$$

The distribution represented by Eq. (4) is defined zero if v is less than v_0. The constant c_z in Eq. (4) is ≈3/2.

A key advantage of coating tungsten (W) with a sodium (Na) sub-monolayer is the significant enhancement in Ps^- production efficiency, which increases from about 0.1% to approximately 1.5% [7]. This surface modification also leads to a notable reduction in the negative work function, consistent with the findings of Kiejna and Wojciechowski [23], who reported that the photoelectric work function of tungsten decreases to around 3 eV after sub-monolayer sodium deposition, attributed to the "surface polarization effect" caused by the alkali metal. Given the functional relationship governing the Ps^- work function, this polarization effect is also expected to influence Ps^- emission. The measured absolute value of the negative work function for Ps^- in polycrystalline or monocrystalline [100]-oriented tungsten without coating is approximately 1 eV. Consequently, it is estimated that this value can reach $\phi \approx 4$ eV when the material is coated with a Na sub-monolayer, resulting in a significant increase in Ps^- emission energy (see Ref. [7]).

The proposed velocity distributions depend solely on the sample temperature and the Ps- work function, requiring no additional parameters. These straightforward expressions can be validated in the future, for instance, using a direction-dependent grating deceleration system. Comparing simulated and experimental data will help determine whether this is the appropriate emission model and beam formation for Ps^- in gravitational studies.

2.2. Ps^- acceleration and optics

Investigation of the initial conditions is crucial to optimize the optical configuration needed to guide and focus the ions to form a coherent Ps^- beam. Initially, a monoenergetic positron beam is implanted in a sodium-coated tungsten (W) sample. This sample operates in transmission geometry, serving as a positron/Ps^- converter. As a result, a cylindrical beam of negative (Ps^-) ions with a diameter of 1 mm is generated. Although Ps^- ions have a limited lifetime of 479 ps, they have the advantage of being influenced by Coulomb forces, allowing for efficient guiding and focusing. The emission of Ps^- ions occurs perpendicular to the converter surface, with a kinetic energy of ≈4 eV as introduced in Section 2.1. A thermal contribution is added according to the sample temperature and following the above proposed velocity distribution.

An electrostatic system with electrodes at different electrical potentials has been developed. The short lifetime of the Ps^- requires the development of an extremely compact electrode design at a sub-millimetric scale. To realize this electrostatic system and reconstruct the Ps^- beam trajectory, a simulation was developed using the SIMION® software. This software calculates the trajectories of charged particles in a region of space where the electric fields are generated. These fields are calculated from geometrically defined electrodes with a set of applied potentials.

This simulation was developed in order to achieve the following goals: (i) accelerate the Ps^- ions to a final kinetic energy of 300 eV, to obtain after photo-detachment an average kinetic energy of 200 eV with Ps; (ii) focus the beam with a minimum divergence given the initial conditions; (iii) develop a compact electrodes design to minimize the Ps^- annihilation. The electrode geometry, designed based on these criteria, is shown in Fig. 1. In particular, Fig. 1(a) gives a schematic representation, not drawn to scale. For a more accurate representation, Fig. 1(b) presents the scaled scheme used for the SIMION® simulation.

The system consists of a positron/Ps^- converter (a monocrystalline Na-coated W sample), a focusing ring, and a grounded electrode with a hole centered in the beam axis. The converter has been idealized as a disk with a radius of 2.5 mm to which a potential of −300 V is applied. This is repulsive for the Ps^- ions which are therefore accelerated towards the grounded electrode to reach 300 eV kinetic energy. A 1 mm diameter hole has been opened in the center of the last electrode to allow the beam to pass through. To avoid propagating electrostatic fields outside this system, this hole has also been closed with a conductive grounded grid. The high transmission grid consists of a series of metal wires (1 μm in diameter) with a pitch of 50 μm.

The distance between this last electrode and the converter is 0.6 mm. This ensures the dielectric strength necessary to avoid electric discharges given the applied potential differences. To better control and reduce the divergence of the beam, a focusing ring with a 2 mm diameter was also inserted in an intermediate position between the two electrodes just described (0.3 mm after the converter). The potential to be applied to this electrode in order to minimize the divergence of the beam is −320 V.

Ps^- ions are generated by the SIMION® simulation from the surface of the converter. Their initial position (x, y) is randomly extracted within a Gaussian distribution centered with the center of the converter and with a standard deviation of 0.2 mm. This simulation provides the electric field configuration necessary for the Monte Carlo simulations.

2.3. Photo-detachment cavity and designed interferometer

Immediately after the last electrode, the Ps^- beam is illuminated by a laser beam propagating along the x-axis to produce a Ps beam via photo-detachment. Two lasers at two different wavelengths were considered for this process: 1560 nm and 3600 nm. The shorter laser wavelength was chosen to be very close to the peak of the photo-detachment cross section [7], while 3600 nm wavelength was studied to reduce broadening due to recoil and excitation. Unfortunately, this option is not feasible in a continuous regime, as proposed in this study. In any case, we are interested in exploring the reduction of the recoil effect at this wavelength for a possible pulsed option system.

The 1560 nm CW laser system consists of an erbium fiber laser coupled with a high finesse Fabry–Pérot enhancement cavity to accumulate a circulating power of about 200 kW. The ultra-low loss mirrors and setup are similar to those used in the PVLAS experiment [24]. Instead, the 3600 nm laser will be a pulsed laser with similar characteristics to Ref. [25].

A Mach–Zehnder interferometer was designed to perform Ps gravity measurements (see Ref. [14]). To complete this gravity measurement in a reasonable time, the interferometer requires a high number of Ps atoms with angles between ±125 μrad and ±170 μrad in y and x-directions respectively. The matter-wave Mach–Zehnder interferometer, located after the optics described in this work, measures the gravitational acceleration through the phase shift induced by a set of light pulses to the Ps wavefunctions in a gravitational field. Compared with a moiré deflectometer, this interferometer has the advantage of being able to work with significantly higher atomic beam speeds since it does not aim to detect the classical deflection of atoms but the interference of atomic wave functions. In addition, it has no grating absorption.

After the photo-detachment cavity at 4.6 mm from the converter, Ps atoms are first excited from the 1^3S_1 level to the 2^3P_0 level by a 243 nm laser then to the 2^3S_1 level by an 18.25 GHz circularly polarized microwave radiation. A similar UV-microwave excitation scheme can be found in Ref. [26]. The 2^3S_1 state has a lifetime of 1.14 μs and allows for relatively long propagation through a Mach–Zehnder interferometer. The atomic wave-function is split in two branches and the internal Ps state oscillates between the 2^3S_1 and 3^3P_2 states due to the interaction with several laser pulses having a wavelength equal to 1312.2 nm. At the interferometer output one of the branches is removed with a laser ionization stage of level 3^3P_2 and two electrodes remove the remaining positrons and electrons to prevent them from contributing to the detected noise. Since the number of atoms exiting one of the two interferometer arms is proportional to the phase shift, it is possible to measure the gravitational acceleration of Ps simply by means of a detector which counts the impinging atoms. The following steps after the photo-detachment are described in detail in Ref. [14], where a simulation of the time needed to measure the gravity acceleration with a precision of 10% is also presented.

2.4. The Monte Carlo simulation

A Monte Carlo simulation was conducted to calculate the trajectories of 10^6 Ps^- ions in the electric field configuration designed with SIMION®. The simulation traced the path of the ions from the converter to the entrance of the Mach–Zehnder interferometer. The path of each ion is computed in every time step (a tenth of a picosecond), linearly interpolating the field. With the aim of comparing the dependence of the final Ps spatial spread on the velocity distribution at two different Ps^- emitting targets temperatures, simulations at room temperature (300 K) and cryo temperature (10 K) were performed. Ps- has never been formed at cryogenic temperature. We propose the hypothesis that Ps- could be formed with the same efficiency as at room temperature. In practical applications, before cryogenically cooling a delicate converter surface (Na coated W) the use of absorption and cryogenic traps to prevent target surface contamination from residual gases will be required.

The Ps^- ions are generated from a disc surface of 1 mm in diameter following a Gaussian distribution. The velocity and direction of Ps^- are obtained adding the three-velocity components v_x, v_y and v_z following the distributions proposed in Section 2.1 (Eqs. (1) and (4)). The simulation considers the realistic conditions that $g_L(v)$ in the z-direction tends to zero when the velocity v is less than v_0 or greater than v_0 plus half the thermal velocity v_{th}, which is given by $v_{th} = \alpha^{-1/2}$ (where α is given by Eq. (2)). The thermal velocity v_{th} is $\sim 10^4$ m/s at 10 K and $\sim$ 5.48×10^4 m/s at 300 K. Instead, the distribution of the transversal velocity $f_T(v)$ tends to zero when the velocity v is greater than 5 times the thermal velocity. The above upper limits for the simulated distributions ensure that the proposed functions given by Eqs. (1) and (4) tend to zero. Fig. 2 displays the velocity distributions of 10^6 Ps^- ions obtained at both 10 K and 300 K. Fig. 2 (a) and (b) illustrates the dependence of the distributions on temperature: if the temperature decreases, the distributions become sharper and the average velocity decreases. These findings reveal the optimum initial conditions to achieve a monochromatic Ps beam before acceleration (Section 2.2). On the other hand, the initial divergence of the beam at low temperature, given by the angular beam aperture $\theta \approx \frac{2v_x}{v_z}$, will be reduced and localized if compared with high room temperature conditions.

After forming, the Ps^- leaves the last electrode grid, reaches its maximum velocity and enters the laser beam for photo-detachment. This process has been included in the simulation and the probability of detachment at each time step is given by:

$$P_{ph} = 1 - \exp\left(-\frac{\lambda\sigma}{hc\overline{P_1P_2}}\int_{t_1}^{t_2}\int_{P_1}^{P_2} I(s,t)\,ds dt\right) \tag{7}$$

where λ is the laser wavelength, σ is the photo-detachment cross section, h is the Planck constant, c is the speed of light and $I(s,t)$ is the laser intensity which is a function of space (s) and time (t). The points P_1 and P_2 define the start and end of the Ps trajectory segment within the laser. Assuming that the optical cavity is along the x-direction and that the laser can be seen by the atomic beam as a standing wave in both the continuous and pulsed regime (long pulses), the intensity takes the form

$$I(x,y,z,t) = 4I_0 \exp\left(\frac{-2(y^2+z^2)}{w_0^2}\right)\cos^2(kx) \tag{8}$$

where w_0 is the minimum laser beam waist.

The integral of intensity is numerically evaluated between the positions of the Ps in its trajectory each time step according to its velocity. When the Ps^- is photo-detached, the recoil of the Ps, due to the absorption of the photon and the one due to the detachment of the electron, are simulated. The absorption of the photon induces a recoil along the laser direction (x-axis) with a positive or negative sign. Given the low energy of the photon, this recoil is negligible compared to the effect of electron detachment.

The two bodies separation recoil depends on the residual energy after breaking the bond between one of the electrons and the newly formed positronium atom and consequently on the wavelength of the photon. This energy is given by the difference between the photon energy of the laser and the photo-detachment threshold which is about 0.327 eV [25].

By setting the linearly polarized electric field of the laser along the z-axis, the angle between the velocity variation caused by the detachment recoil and the z-axis has a "cosine-squared" distribution so that

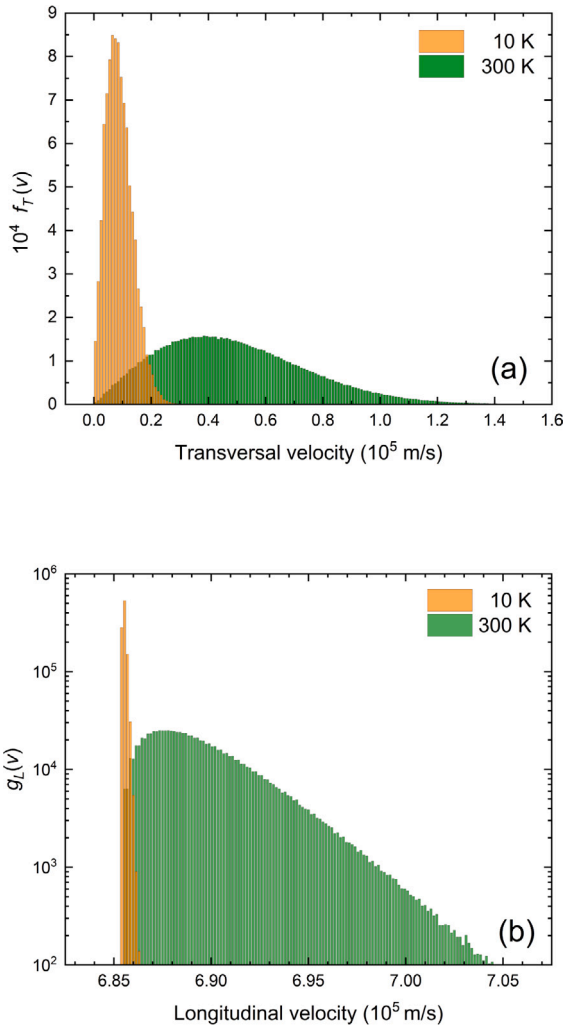

Fig. 2. (a) Transversal velocity distribution in the x or y-directions. (b) Longitudinal velocity distribution in the z-direction. Both distributions are obtained at two different Ps^- emitting targets temperatures (10 K and 300 K) by Monte Carlo simulations following the proposed Eqs. (1) and (4), respectively. The $g_L(v)$ distribution is presented in logarithmic scale to improve the visualization.

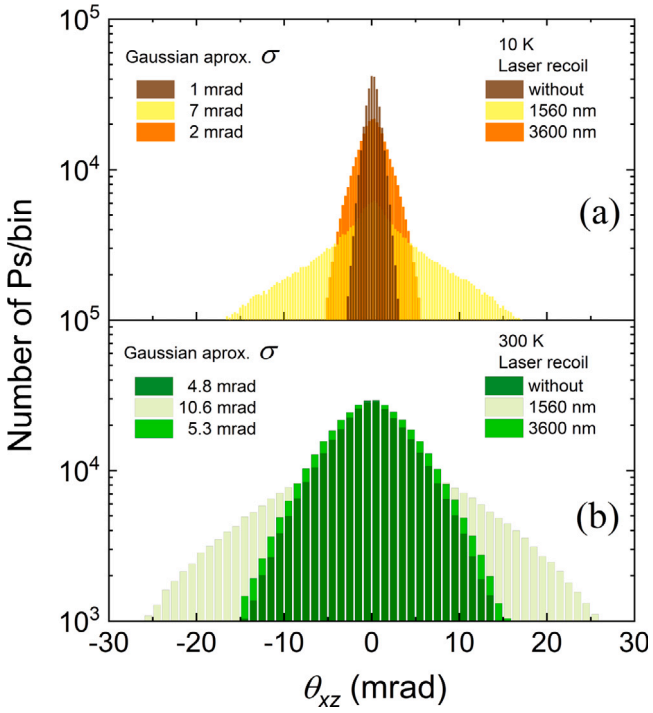

Fig. 3. Angular distributions θ_{xz} of Ps after laser recoil during photo-detachment obtained via Monte Carlo simulations. The angular distributions θ_{yz} are almost identical to the θ_{xz}, the possible differences are within computational error. Results obtained for two different Ps^- emitting targets temperatures: at 10 K in (a) and at 300 K in (b).

the most probable values are close to zero. The distribution of the angle between the x-y plane velocity projection and the y-axis is uniform in all directions [6,27]. This recoil effect has recently been verified by using linearly polarized light in a Ps^- laser photo-detachment scheme also showing that it is well described by the theory of Photoelectrons Angular Distributions (PAD) [27,28] with an asymmetry parameter equal to 2 [29].

One way to avoid this effect is to use a laser having energy close to the photo-detachment threshold energy, which corresponds to a wavelength of about 3800 nm. This wavelength region is achievable at high power only in the pulsed regime, and the cross-section is about one order of magnitude smaller than the maximum with a laser of 1560 nm [7]; this implies that a laser power higher than 200 kW is required to keep the photo-detachment efficiency high. A 3600 nm pulsed laser system can reach 2 MW with high repetition rate [30] and can then replace the CW 1560 nm laser. Using the 3600 nm laser, the effect of photo-detachment on beam divergence is minimized.

The plots in Fig. 3 represent the Ps angular distributions $\theta_{xz} = \arctan\left(\frac{v_x}{v_z}\right)$ for Ps^- emitting targets at T = 10 K and T = 300 K. The distribution in the perpendicular direction θ_{YZ} is almost identical to θ_{xz}, the possible differences are within computational error. The dominant effect of recoil in this scenario is the electron detachment. Since this effect occurs in a random direction, it equally impacts the θ_{yz} and θ_{xz} distributions, resulting in a similar heating effect on the Ps beam.

A hypothetical recoilless distribution for an "ideal" laser is also included in Fig. 3 to visualize the electron detachment effect in the Ps beam. The distributions follow a Gaussian-like trend. On the left of Fig. 3 (a) and (b) the approximate standard deviation σ of the distributions (affected with an error ± 0.2 mrad) is shown to compare the influence of the laser recoil on the width of each profile as a function of the wavelength (1560 nm and 3600 nm). The distributions for Ps^- emitting targets at 10 K and 300 K follow a similar pattern. The 3600 nm wavelength minimizes the laser recoil effect, especially when the Ps^- emitting target is at room temperature (300 K).

With this setup, the effect of recoil is to broaden the angular distribution of the Ps beam mainly in the z-direction, while minimizing its divergence in the x and y directions. This choice is particularly convenient since the interferometer is more sensitive to x and y broadening than the broadening in z-direction.

Fig. 4 shows the spread in kinetic energy in the z-direction after the laser recoil during photo-detachment. The results demonstrate that the Ps energy spread mainly depends on the laser wavelength, the influence of the Ps^- emitting targets temperature is almost negligible in the z-direction. The net effect in this direction is to produce a symmetric spread in energy of about ± 12%, when the 1560 nm laser is used, instead the spread is minimized up to approximately ± 2% using the 3600 nm laser for the photo-detachment. Following the simulations presented in Ref. [14] the z broadening effect reduces only few percent of the interferometer efficiency and results in being non-critical.

To make a comparison, both the lasers at 1560 nm and 3600 nm have been simulated. After crossing the laser beam, the positions and velocity components of the atoms that survived annihilation are stored and analyzed. Only the Ps in a 0.4 cm x 0.4 cm area are considered, in line with the angular divergence criteria requested in Ref. [14]. The distance between the converter and the excitation stage is 4.6 mm

Table 1
Monte Carlo statistics in percentage of the number of Ps^- emitted for various simulation steps. The columns are for the four combined alternatives of laser wavelength and temperature. The standard error is given in parentheses. The number of Ps^- emitted by the target is 1 million under all initial conditions.

Laser wavelength	1560 nm	1560 nm	3600 nm	3600 nm
Temperature	10 K	300 K	10 K	300 K
Ps^- decayed before the laser (%)	32.72 (0.04)	32.70 (0.04)	32.72 (0.04)	32.70 (0.04)
Ps^- decayed in the laser (%)	33.17 (0.06)	32.43 (0.06)	30.17 (0.05)	28.85 (0.05)
Ps^- arrived at the laser (%)	34.11 (0.05)	34.87 (0.04)	37.12 (0.03)	38.46 (0.03)
Ps^- detached by the laser (%)	32.51 (0.04)	33.75 (0.04)	36.25 (0.03)	38.22 (0.04)
Ps decayed in the laser (%)	0.020 (0.001)	0.020 (0.001)	0.030 (0.001)	0.030 (0.001)
Laser photo-detach. efficiency (%)	95 (1)	97 (1)	98 (1)	99 (1)
Ps entering the Mach–Zehnder interferometer (%)	32.49 (0.04)	33.73 (0.04)	36.23 (0.03)	38.20 (0.04)
Ps with θ_{xz} lower than 170 μrad (%)	0.688 (0.009)	0.446 (0.003)	2.422 (0.016)	0.963 (0.014)
Ps with θ_{yz} lower than 125 μrad (%)	0.516 (0.010)	0.332 (0.004)	1.830 (0.020)	0.729 (0.009)
Ps inside θ_{yz} and θ_{xz} (125 μrad × 170 μrad) (%)	0.028 (0.002)	0.005 (0.001)	0.155 (0.005)	0.022 (0.001)

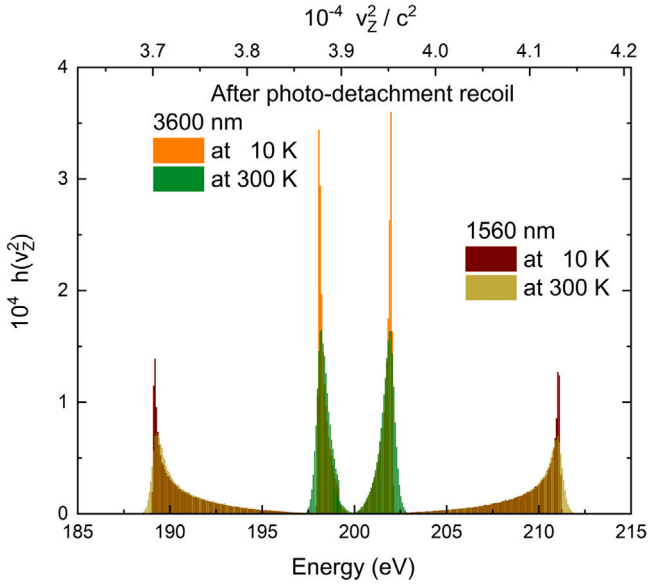

Fig. 4. Ps energy distribution h (multiplied by a factor 10^4) after the photo-detachment recoil in z-direction. The distributions are symmetric compared to the Ps average kinetic energy (200 eV). The recoil effect is simulated for two different photo-detachment laser wavelengths, 1560 nm and 3600 nm, and two Ps^- emitting targets temperatures, 10 K and 300 K.

(see Fig. 1(b)). The results of the Monte Carlo simulation presented here for the laser wavelength 1560 nm and 3600 nm and for two Ps^- emitting targets temperatures (10 K and 300 K) are shown in Table 1. The results indicate that after the emission of 10^6 Ps^- around 33% and 37% on average reach the Mach–Zehnder interferometer entrance for the 1560 nm and 3600 nm lasers, respectively. Now the most relevant limitation is the divergence tolerance of the interferometer of the order of a hundred of microradians (±125 μrad and ±170 μrad in y and x-directions). The last three rows of Table 1 show the efficiency in the x and y-direction and the efficiency of the overall in both directions. The best efficiencies were achieved by using the 3600 nm laser, especially when the Ps^- emitting target is at cryogenic temperature.

Monte Carlo simulations are subject to various sources of error, including statistical uncertainties and systematic errors originating from several factors. Here, potential systematic errors were idealized and minimized. A detailed discussion of these errors will be made in due course, providing more insight into the experimental conditions governing the formation of the Ps beam. For instance, an assessment of this error source could be conducted by considering the uncertainty in the field distribution guiding the Ps^- beam and the conditions pertaining to Ps-laser interaction during photo-detachment, among other factors. Regarding error sources, the brackets in Table 1 encompass the estimated standard errors in the results for each temperature and laser. These errors were evaluated through ten simulation runs with different seeds, and the average value of the results was calculated. The results follow a Poisson distribution, where median and media are almost the same and the skewness is between −2 and 2 in all four cases presented in Table 1.

Following the methodology proposed in Ref. [14], it is necessary to consider a very bright positron beam to perform interferometric measurements of Ps gravity on the time scale of the year. We propose to use a LINAC as primary electron beam to produce positron–electron pairs. For instance, the Milan BriXSinO (Brilliant source of X-rays based on Sustainable and innOvative accelerators) facility proposes a superconductive LINAC operating at 92 MHz with an average electron current of 2–5 mA, an acceleration energy of 10 MeV [31–33]. At least 5×10^{16} fast electrons per second will be produced with this kind of LINAC with a beam spot lower than 1 mm and very small divergence of about 50 μrad. These excellent characteristics allow us to predict a high e^+/e^- conversion efficiency, in particular using an efficient positron moderator, such as tungsten meshes, a total conversion efficiency (cold e^+)/(hot e^-) of at least 10^{-5}-10^{-6} is expected [34]. These characteristics can be compared with the performance of other LINAC-based positron sources in Ref. [34]. The positron rate expectation of the slow beam is of around 10^9-10^{10} positrons per second with the technical conditions mentioned above. Considering a conversion efficiency of the target converter (tungsten decorated with sodium) for Ps^-/e^+ is around 10^{-2} in transmission and in reflection [7,35], our expectation is to obtain 10^7-10^8 Ps^- per second emitted from the target. In contrast, using a LINAC as presented in Ref. [34] our expectation is to obtain 10^5-10^6 Ps^- per second.

We propose implementing a periodic exchange of the e^+/Ps^- converter, followed by a thermal treatment at high temperature (at about 2300 K) to remove impurities and possible damages followed by the deposition of fresh sodium on the tungsten surface.

These simulations are conducted using a Gaussian Ps^- beam profile based on a standard positron beam dimension of 1 mm diameter (detailed in Section 2.2). However, an alternative approach, as described in Ref. [36], allows remoderation of the primary positron beam, resulting in a beam with a diameter one order of magnitude smaller [37]. Nevertheless, this option also leads to reduced positron statistics of one order of magnitude. Despite the trade-off, the reshaping approach increases the positron density at the center of the distribution, thereby improving the final Ps statistics relevant for Mach–Zehnder interferometry. Consequently, remoderation facilitates an increase in the statistical significance of recorded events and a reduction in data acquisition time. Additional investigation and a comprehensive study will be undertaken to evaluate the feasibility and benefits of these approaches.

2.5. Conclusions

This work reports the Monte Carlo simulation of a Ps beam that can be applied to perform gravity measurement by using a Mach–Zehnder interferometer proposed in Ref. [14]. The main results are presented below:

- Utilizing a primary Ps^- ion beam enables the creation of a continuous high-statistic, low-divergence, and monoenergetic Ps beam.
- A distribution of the initial velocity of the Ps negative ion primary beam, originating from the positron/Ps^--converter, has been proposed, considering parameters such as the Ps^- thermalization temperature. This distribution has been estimated at temperatures of 10 K and 300 K.
- The specifications of the system essential for generating the Ps beam have been defined with a view towards potential optimization. The angular dispersion of the beam at the proposed kinetic energy (200 eV) is primarily affected by laser interaction during photo-detachment. The quantity of Ps atoms accepted by the Mach–Zehnder interferometer, within divergences of $\pm 125\,\mu$rad and $\pm 170\,\mu$rad in the y and x directions, respectively, has been estimated.

The advantage of the approach presented above compared to other methods for Ps formation is that the primary Ps^- ion beam can be accelerated, focused and guided. By then using a high-finesse laser cavity it is possible to photo-detach the extra electron and form Ps. Two different laser wavelengths were proposed. One is a CW cavity of 1560 nm and the other is a pulsed laser of 3600 nm. The latter minimizes beam spread, but requires modifying the strategy of a continuous beam and implementing a pulsed system. The statistical findings from this study underscore the necessity for a robust source of bright positron beams to generate the requisite Ps flux.

CRediT authorship contribution statement

M. Sacerdoti: Writing – original draft, Software, Formal analysis, Data curation. **V. Toso:** Writing – review & editing, Validation, Software, Investigation, Formal analysis, Data curation. **G. Vinelli:** Writing – original draft, Methodology, Investigation, Formal analysis. **M. Bayo:** Writing – review & editing, Investigation. **G. Rosi:** Writing – original draft, Visualization, Validation, Investigation, Conceptualization. **L. Salvi:** Writing – review & editing, Supervision, Investigation. **G.M. Tino:** Writing – review & editing, Supervision, Investigation. **M. Giammarchi:** Writing – review & editing, Validation, Project administration, Funding acquisition. **R. Ferragut:** Writing – original draft, Supervision, Methodology, Data curation, Conceptualization.

Declaration of competing interest

The authors declare the following financial interests/personal relationships which may be considered as potential competing interests: Rafael Ferragut reports financial support and administrative support were provided by Politecnico di Milano. All the authors reports financial support and equipment, drugs, or supplies were provided by National Institute of Nuclear Physics. If there are other authors, they declare that they have no known competing financial interests or personal relationships that could have appeared to influence the work reported in this paper.

Acknowledgments

The authors thank Istituto Nazionale di Fisica Nucleare, Italy (CSN 3) and Politecnico di Milano, Italy for support.

Data availability

Data will be made available on request.

References

[1] D. Colladay, V.A. Kostelecký, CPT violation and the standard model, Phys. Rev. D 55 (1997) 6760–6774.
[2] D. Colladay, V.A. Kostelecký, Lorentz-violating extension of the standard model, Phys. Rev. D 58 (1998) 116002.
[3] E.K. Anderson, et al., ALPHA Collaboration Collaboration, Observation of the effect of gravity on the motion of antimatter, Nature 621 (2023) 716–722.
[4] V.A. Kostelecký, A.J. Vargas, Lorentz and CPT tests with hydrogen, antihydrogen, and related systems, Phys. Rev. D 92 (2015) 056002.
[5] R. Mikami, Y. Nagata, Y. Sada, Y. Nagashima, Positronium transmission through graphene thin films supported with lacy carbon in the energy range of a few kev, Eur. Phys. J. D 77 (2023) 25.
[6] K. Michishio, L. Chiari, F. Tanaka, N. Oshima, Y. Nagashima, A high-quality and energy-tunable positronium beam system employing a trap-based positron beam, Rev. Sci. Instrum. 90 (2) (2019) 023305.
[7] Y. Nagashima, Experiments on positronium negative ions, Phys. Rep. 545 (3) (2014) 95–123.
[8] G. Consolati, R. Ferragut, A. Galarneau, F. Di Renzo, F. Quasso, Mesoporous materials for antihydrogen production, Chem. Soc. Rev. 42 (2013) 3821–3832.
[9] S. Aghion, et al., AEgIS Collaboration Collaboration, Producing long-lived 2^3S positronium via 3^3P laser excitation in magnetic and electric fields, Phys. Rev. A 98 (2018) 013402.
[10] P. Crivelli, U. Gendotti, A. Rubbia, L. Liszkay, P. Perez, C. Corbel, Measurement of the orthopositronium confinement energy in mesoporous thin films, Phys. Rev. A 81 (2010) 052703.
[11] H. Ceeh, C. Hugenschmidt, K. Schreckenbach, S.A. Gärtner, P.G. Thirolf, S.M. Fleischer, D. Schwalm, Precision measurement of the decay rate of the negative positronium ion Ps^-, Phys. Rev. A 84 (2011) 062508.
[12] G.M. Tino, Testing gravity with cold atom interferometry: results and prospects, Quantum Sci. Technol. 6 (2) (2021) 024014.
[13] G.M. Tino, M.A. Kasevich (Eds.), Atom Interferometry, SIF and IOS Press, 2014.
[14] G. Vinelli, F. Castelli, R. Ferragut, M. Romé, M.G. Sacerdoti, L. Salvi, V. Toso, M.G. Giammarchi, G. Rosi, G.M. Tino, A large-momentum-transfer matter-wave interferometer to measure the effect of gravity on positronium, Classical Quantum Gravity 40 (20) (2023) 205024.
[15] R.M. Nieminen, J. Oliva, Theory of positronium formation and positron emission at metal surfaces, Phys. Rev. B 22 (1980) 2226–2247.
[16] H. Zhang, T. Pincelli, C. Jozwiak, T. Kondo, R. Ernstorfer, T. Sato, S. Zhou, Angle-resolved photoemission spectroscopy, Nat. Rev. Methods Primers 2 (1) (2022) 54.
[17] D.M. Chen, S. Berko, K.F. Canter, K.G. Lynn, A.P. Mills, L.O. Roellig, P. Sferlazzo, M. Weinert, R.N. West, Angle-resolved positronium emission spectroscopy, Phys. Rev. Lett. 58 (1987) 921–924.
[18] A. Kawasuso, M. Maekawa, A. Miyashita, K. Wada, Y. Nagashima, A. Ishida, Positronium emission from GaN(0001) and AlN(0001) surfaces, J. Phys. B: At. Mol. Opt. Phys. 54 (20) (2021) 205202.
[19] A.P. Mills, L. Pfeiffer, Desorption of surface positrons: A source of free positronium at thermal velocities, Phys. Rev. Lett. 43 (1979) 1961–1964.
[20] K. Sudarshan, S.N. Samarin, P. Guagliardo, V.N. Petrov, A.H. Weiss, J.F. Williams, Angle-resolved energy distribution of re-emitted positrons from a W(100) single crystal, Phys. Rev. B 87 (2013) 085418.
[21] C.A. Murray, A.P. Mills, Narrow beam emission of slow positrons from negative affinity surfaces, Solid State Commun. 34 (10) (1980) 789–794.
[22] D.A. Fischer, K.G. Lynn, D.W. Gidley, High-resolution angle-resolved positron reemission spectra from metal surfaces, Phys. Rev. B 33 (1986) 4479–4492.
[23] A. Kiejna, K. Wojciechowski, Work function of metals: Relation between theory and experiment, Prog. Surf. Sci. 11 (4) (1981) 293–338.
[24] A. Ejlli, F. Della Valle, U. Gastaldi, G. Messineo, R. Pengo, G. Ruoso, G. Zavattini, The PVLAS experiment: A 25 year effort to measure vacuum magnetic birefringence, Phys. Rep. 871 (2020) 1–74.
[25] K. Michishio, S. Kuma, Y. Nagata, L. Chiari, T. Iizuka, R. Mikami, T. Azuma, Y. Nagashima, Threshold photodetachment spectroscopy of the positronium negative ion, Phys. Rev. Lett. 125 (2020) 063001.
[26] L. Gurung, T.J. Babij, S.D. Hogan, D.B. Cassidy, Precision microwave spectroscopy of the positronium $n = 2$ fine structure, Phys. Rev. Lett. 125 (2020) 073002.
[27] J. Cooper, R.N. Zare, Angular distribution of photoelectrons, J. Chem. Phys. 48 (2) (1968) 942–943.
[28] V. Davis, Introduction to Photoelectron Angular Distributions: Theory and Applications, Springer International Publishing, 2022.
[29] K. Michishio, L. Chiari, F. Tanaka, Y. Nagashima, Anisotropic photodetachment of positronium negative ions with linearly polarized light, Phys. Rev. Lett. 132 (2024) 203001.

[30] X. Li, X. Huang, X. Hu, X. Guo, Y. Han, Recent progress on mid-infrared pulsed fiber lasers and the applications, Opt. Laser Technol. 158 (2023) 108898.
[31] A. Bacci, et al., TDR BriXSinO, Technical Report, Istituto Nazionale di Fisica Nucleare, 2022.
[32] I. Drebot, et al., BriXSinO high-flux dual X-Ray and THz radiation source based on energy recovery Linacs, in: Proc. IPAC 22, in: International Particle Accelerator Conference, (no. 13) JACoW Publishing, Geneva, Switzerland, 2022, pp. 2407–2410.
[33] A. Bacci, F. Broggi, V. Petrillo, L. Serafini, Low emittance positron beam generation: A comparison between photo-production and electro-production, 2021.
[34] M. Charlton, et al., Positron production using a 9 MeV electron linac for the GBAR experiment, Nucl. Instrum. Methods Phys. Res. A: Accel. Spectrom. Detect. Assoc. Equip. 985 (2021) 164657.
[35] Y. Nagashima, Personal communication, 2023.
[36] P.J. Schultz, E.M. Gullikson, A.P. Mills, Transmitted positron reemission from a thin single-crystal Ni(100) foil, Phys. Rev. B 34 (1986) 442–444.
[37] T. Gigl, L. Beddrich, M. Dickmann, B. Rienäcker, M. Thalmayr, S. Vohburger, C. Hugenschmidt, Defect imaging and detection of precipitates using a new scanning positron microbeam, New J. Phys. 19 (12) (2017) 123007.